THE JOURNAL OF PHYSICAL CHEMISTRY Letters

Letter

pubs.acs.org/JPCL

Hierarchical Photonic Synthesis of Hybrid Nanoparticle Assemblies

Zijie Yan,[†] Uttam Manna,[†] Wei Qin,[†] Art Camire,[§] Philippe Guyot-Sionnest,[†,‡] and Norbert F. Scherer*[,†]

[†]The James Franck Institute and Department of Chemistry and [‡]Department of Physics, The University of Chicago, 929 East 57th Street, Chicago, Illinois 60637, United States

[§]Spectra-Physics Laser Division, Newport Corporation, 3635 Peterson Way, Santa Clara, California 95054, United States

Supporting Information

ABSTRACT: Optical "nano-manipulation" to control small objects with nanoscale precision requires strongly localized optical fields that are usually based on user-imposed shaping of the incident optical beam. Here we report an in situ approach to reshape and enhance electromagnetic (EM) fields using scattering and interference that is concomitant with "dynamic self-assembly" of nanoparticle arrays using simple (unstructured) applied EM fields. We show that Ag nanoparticles (~140 nm diameter) illuminated by coherent light can form linear chains with nanometer precision via strong optical binding interactions. The chains, in turn, create highly shaped EM fields via coherent scattering from the particles, allowing less polarizable particles to be "co-trapped" in both intermediate-scale and near-field regimes. These less polarizable particles include quantum dots (CdSe/ZnS or CdSe/CdZnS core/shell nanocrystals; both are smaller than 10 nm, while the latter are further coated by ~30 nm thick silica shells) and small Ag nanoparticles (60 nm diameter). This hierarchical optical-field-induced assembly is a starting point for photonically building artificial nanomaterials.

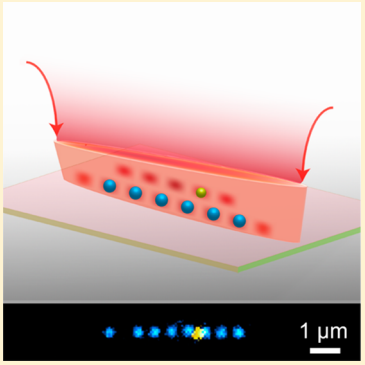

SECTION: Plasmonics, Optical Materials, and Hard Matter

Control over the chemical interactions between nanoparticles has recently led to the formation of new heterostructures and even quasi-crystals.[1,2] Photonic interactions have lead to the creation of cold atom lattices.[3] Furthermore, optical forces have become a powerful noncontact approach for studying individual nanoparticles and biomolecules.[4−6] Yet, using light to simultaneously control and assemble multiple nanoparticles into ordered arrays is still challenging. Strongly localized (or focused) optical fields are usually required for optical manipulation.[7] The regimes for this manipulation can be classified into far-field ($d \gg \lambda$), intermediate-field ($d \approx \lambda$), and near-field ($d \ll \lambda$). A widely used far-field technique is the traditional optical tweezers[8] with a tightly focused Gaussian beam. Integration of spatial light modulators with optical tweezers has enabled the production of structured light fields for advanced manipulation.[9−11] Still, far-field light shaping is limited by diffraction. Near-field techniques based on user-imposed light shaping overcome the diffraction limit[12−14] yet usually require ex situ fabrication of designed trapping devices. Subwavelength manipulation by evanescent light fields has recently been demonstrated,[15,16] and plasmonic tweezers,[13,14,17−19] a near-field technique, has attracted much attention. In the latter, the plasmon resonance of noble-metal structures with nanometer-scale features can strongly enhance the EM fields near the metal surface and thus create localized EM fields. These far-field and near-field techniques are being widely applied in nanoscience and biology.[4,5,12,20]

Exciting opportunities will emerge from shaping EM fields in the intermediate-scale region, including strong coupling of photon sources to nanophotonic systems and assembling hybrid photonic architectures.[21] One approach involves optical trapping by light shaping and focusing in fabricated photonic lattices.[12,22] The light−matter interaction termed "optical binding"[23] is another approach to shape light in the intermediate-scale regime and has the potential to create dynamically reconfigurable structures. Optical binding of micrometer or submicrometer dielectric (e.g., polymer) beads occurs when the scattered light from these beads interferes with the incident field, resulting in field gradients and thus spatial arrangement of the beads.[24,25] The process of array formation by the optical binding interaction in the presence of a continuous applied EM field is a type of "dynamic self-assembly".[26] Metal particles are stronger light scatterers (per volume) than polymer particles, allowing strong optical binding of Au nanoparticle pairs,[27,28] and optical binding interaction of Ag nanoparticles as small as 40 nm in diameter has recently been demonstrated.[29]

Here we report that chains of large Ag nanoparticles (~140 nm diameter) formed by optical binding interactions can serve as an in situ beam shaper to create localized optical fields and that these nanoparticles and the structured fields they produce can serve as backbones for hierarchical assembly of hybrid nanostructures. The chains assemble in a simple (initially unstructured) optical field and behave as rigid bodies. However,

Received: May 14, 2013
Accepted: July 22, 2013

   dx.doi.org/10.1021/jz401007t | J. Phys. Chem. Lett. 2013, 4, 2630−2636

because the fields scattered from the nanoparticles are coherent and the resulting superposition field has contributions from every particle,[24] the interference creates strong and localized enhanced EM fields near the chain. We show that these localized EM fields are able to "co-trap" small and less polarizable nanoparticles such as semiconductor quantum dots (QDs) and much smaller Ag nanoparticles. As a result, hybrid nanoparticle assemblies are generated by this hierarchical "photonic synthesis".

Hierarchical photonic synthesis of hybrid nanostructures was demonstrated using an optical tweezers apparatus illustrated in Scheme 1. An optical line trap was used to confine multiple Ag nanoparticles (140 ± 30 nm diameter; see Supporting Information, Figure S1) in solution near the surface of a coverslip. These Ag nanoparticles assembled into a linear chain with nearly constant separations (average value of 564 nm) due to strong optical binding forces. Water-soluble QDs (CdSe/ZnS or CdSe/CdZnS/SiO_2) or smaller Ag nanoparticles (60 nm diameter) were also mixed with the 140 nm Ag nanoparticles in solution. The QDs were imaged with spectral discrimination (dichroic mirror in the Dual View), while the small Ag nanoparticles were identified by their weak optical scattering. As illustrated in Scheme 1, each recorded frame from the CMOS array detector contains two regions: the left region only records the orange/red fluorescence from the QDs, and the right side only records the dark-field scattered green light from the Ag nanoparticles. The spatial registration of the two regions was calibrated using white light (i.e., by removing the filter F1) to illuminate the Ag so the same Ag nanoparticles appear in both regions of the detector and the position difference can be used as a reference for precise correlation of the images.[30] When thus calibrated, each frame of the 2-color video provides directly comparable dynamics and spatial (structural) information.

A representative example of the dual spectral-detection imaging is shown in Figure 1a (Supporting Information, Movie S1; the fluctuations in fluorescence intensity of the QD arise from the typical blinking behavior as well as fluctuations in the various particle positions and the alternation of the field enhancement). At 2.7 s of a trapping event, a chain of five Ag nanoparticles was assembled in the optical line trap, and a CdSe/ZnS QD was co-trapped with the Ag particle chain. Images of the Ag particle chain at selected times are shown in Figure 1b. The image at 39.9 s is presented in false color for illustration; we combined the simultaneously recorded locations of QD and Ag particles (cyan for Ag particles and red for QD). Figure 1c shows trajectories of the x positions of the QD and Ag particles in the chain. The averaged positions of the central particles (#2−4) at each time (i.e., frame of the video) were subtracted from the trajectories. This allows us to remove highly correlated motion (noise) of the chain that occurs; that is, the chain behaves as a rigid body (i.e., center of mass motions). The positions of the Ag nanoparticles were determined by strong optical binding forces with inter-particle separations close to the wavelength of the trapping laser in water (λ = 600 nm).[29] The whole chain was fluctuating along its long axis, but the separations between adjacent Ag nanoparticles in the center of the chain were nearly constant. The particles at the ends of the chain exhibit jumps to the second or third nearest optical binding positions. The standard deviation, σ, of the separation between adjacent particles is typically 10 nm for the central pairs and 20 nm for the terminal pairs (see Supporting Information, Figure S2). We can determine the spring constant, κ, resulting from the optical binding interaction using the equipartition theorem $\kappa = 4k_BT/\sigma^2$,[27] where k_B is Boltzmann's constant and T is absolute temperature. The spring constant is 162 pN/μm for optical binding of the central pairs and 41 pN/μm for the terminal pairs. These values are much larger than the recently reported "ultrastrong" optical binding between two 200 nm Au nanoparticles ($\kappa \approx$ 12 pN/μm).[27] The stronger optical binding for spherical Ag nanoparticles versus Au is consistent with the large scattering cross-section and smaller absorption coefficient of Ag at 800 nm.[31]

The trajectory of the QD in Figure 1c can be classified into two behaviors: initially, the QD had nearly the same x positions as Ag particles #4 or 5; later, starting at 33.8 s (when the seventh Ag particle joined the chain), the QD hopped more erratically between the Ag particles #4−7 (e.g., it is shown to be between particles #5 and 6 in the image at 39.9 s in Figure 1b). The chain also became unstable when the eighth Ag particle joined; the reason for instability of a long chain and its influence on co-trapping of QDs are discussed in the Supporting Information. The distributions of positions of the QD shown in Figure 1d indicate that there are two classes of enhanced optical fields created by the chain. Panel I shows that the QD preferred positions close to two Ag particles (in both the x and y directions). We refer to this close proximity localization as "near-field co-trapping". Panel II shows that the same QD later preferred positions between two Ag particles (along the x direction). We refer to localization between the Ag nanoparticles as "intermediate-scale co-trapping". Note that because the two terminal particles each fluctuated between three optical binding positions, the two panels actually show more spots along the x direction compared with the numbers of Ag particles (six in panel I and eight in II). In our experiments, near-field co-trapping was observed more often than intermediate-scale co-trapping, indicating that the EM fields in the former are stronger than those in the latter. For both

Scheme 1. Experimental Setup Used for Creating and Imaging Linear Chains of Optically Bound Ag Nanoparticles and Co-trapping of QDs[a]

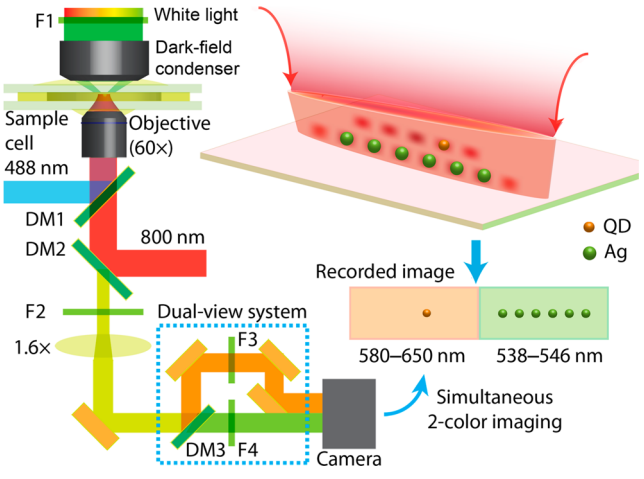

[a]Several dichroic mirrors (DMs) and filters (F's) are used to permit short-pass (SP), long-pass (LP), or band-pass (BP) of the incident light: DM1-LP 538 nm, DM2-SP 770 nm, DM3-SP 665 nm, F1 = BP 530 ± 30 nm, F2 = SP 650 nm, F3 = LP 580 nm, and F4 = BP 542 ± 4 nm.

dx.doi.org/10.1021/jz401007t | J. Phys. Chem. Lett. 2013, 4, 2630−2636

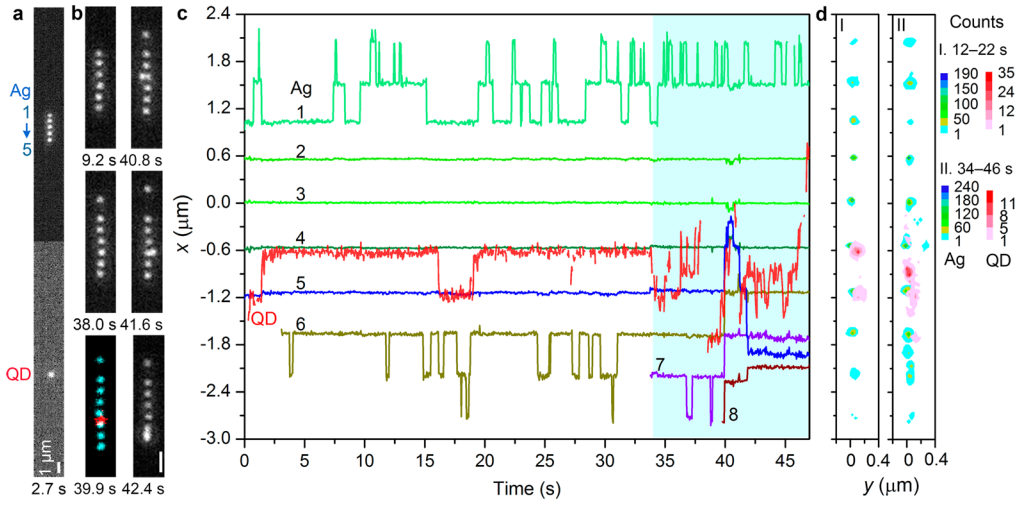

Figure 1. Co-trapping of a CdSe/ZnS QD in a chain of 140 nm Ag nanoparticles formed by optical binding in an optical line trap. (a) Optical image of the QD and Ag nanoparticles recorded by dual spectral-detection imaging. (b) Representative images of the Ag particles at several time points. (c) Trajectories of the QD and Ag particles in the chain. (d) Contour plots of position distributions of the QD and Ag particles in two representative time periods. The unit size for the 2D histograms is 41 × 41 nm^2.

kinds of co-trapping, longer chains were always more effective than shorter chains. (See the Supporting Information, Movie S2 and Figure S3, where the chain began with three Ag nanoparticles, and only when the fifth particle joined was near-field co-trapping of a QD observed.)

Because the maximum gradient force of optical trapping is proportional to the polarizability of a Rayleigh particle, increasing the polarizability of the QDs (e.g., adding material by coating a silica shell around the QD core) enhances the intermediate-scale co-trapping. Figure 2 shows the results of co-trapping a CdSe/CdZnS/SiO_2 QD in a chain of seven Ag nanoparticles (Supporting Information, Movie S3). The Ag

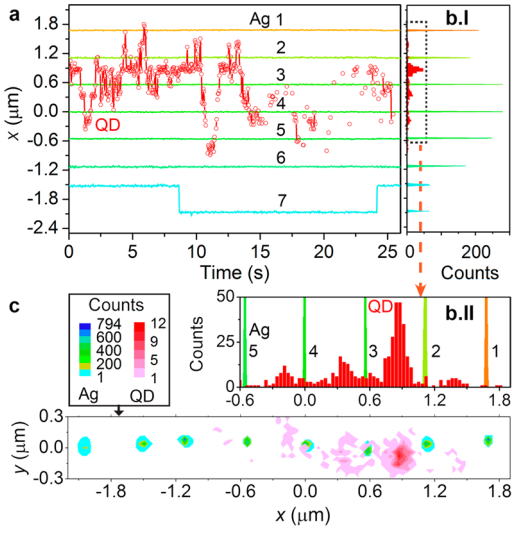

Figure 2. Intermediate-scale co-trapping of a CdSe/CdZnS/SiO_2 QD in a chain of seven Ag nanoparticles. (a) Trajectories of the QD and Ag particles in the chain. The average position of the three Ag particles in the central area (e.g., those with x positions at ∼0 and ±0.6 μm) is defined as a reference at each time. (b) (I) Corresponding histogram of the x positions of the QD and Ag particles and (II) a magnified region of the histogram highlighting the QD distribution. (c) Contour plots of position distributions of the QD and Ag particles. The unit size for the 2D histogram is 41 × 41 nm^2.

particle chain was very rigid, with only one terminal particle jumping twice between two trapping positions (Figure 2a). A QD's location fluctuated in the chain but generally remained between the Ag particles (intermediate-scale co-trapping), as indicated in Figure 2b,c.

As an important control, we found that neither of the two kinds of QDs used in our experiments could be trapped by the optical line trap without Ag nanoparticles. However, they could be trapped by a focused Gaussian beam (e.g., 50 mW average power vs 100 mW for Figures 1 and 2), as has been reported by others.[32] We can also determine the spring constant of co-trapping using the equipartition theorem (we assume the trapped QD is bound to the nearest Ag nanoparticle and assume 4 degrees of freedom[27]). In Figure 1, the standard deviation of the separation between the QD and Ag 4 is 44 nm in the near-field regime. In Figure 2, the standard deviation of the separation between the QD and Ag 2 is 75 nm in the intermediate-scale regime. These values give a spring constant of ∼8 pN/μm for the near-field co-trapping and ∼3 pN/μm for the intermediate-scale co-trapping. These spring constants are larger than that measured from the optical trapping of QDs by a focused Gaussian beam.[32] Therefore, we conclude that the chains of Ag nanoparticles in the optical line trap have created localized EM fields with enhanced intensities that make the co-trapping possible.

We also found that the near-field and intermediate-scale co-trapping readily occurs for smaller Ag nanoparticles. Figure 3a shows several representative optical images of a trapping event involving a 60 nm Ag nanoparticle (termed Ag-s) and several 140 nm Ag nanoparticles (Supporting Information, Movie S4). Trajectories of all particles are shown in Figure 3b. The complexity of the dynamics did not allow subtraction of a center of mass motion of the chain. However, a great deal of the positional noise is highly correlated, reflecting the rigidity of the chain and particle interactions that are large compared with k_BT. Three types of co-trapping behaviors are observed. In type i, the Ag-s nanoparticle was co-trapped in the intermediate-scale region (e.g., at 4 and 20 s), where its x position was between two adjacent large Ag particles. In type ii, normal optical binding occurred between the small and large particles, where

dx.doi.org/10.1021/jz401007t | J. Phys. Chem. Lett. 2013, 4, 2630−2636

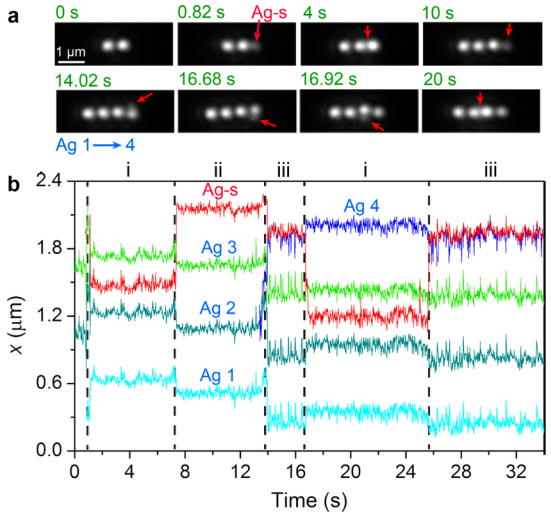

Figure 3. Co-trapping of a smaller Ag nanoparticle (Ag-s, 60 nm diameter) in a chain of larger Ag nanoparticles (140 ± 30 nm diameter). (a) Representative optical images at several times. The small Ag nanoparticle (Ag-s) is much dimmer (i.e., scatters less light) than the larger 140 nm nanoparticles; the positions of Ag-s are indicated by red arrows. (b) Trajectories of all Ag particles in the chain. Three types of co-trapping are shown in panel b: (i) intermediate-scale co-trapping; (ii) optical binding at the canonical optical binding "lattice" spacing; and (iii) an orbital double occupation of a lattice site (along the chain axis).

the Ag-s particle occupied the vacancies of the nearest-neighbor optical binding sites, as defined by the large particles (e.g., at 10 s; see Supporting Information, Movie S5 and Figure S4 for another example). A similar optical binding behavior was also observed by Demergis et al.,[27] where trapping of a small Au nanoparticle (100 nm diameter) was assisted by the optical binding forces between larger Au nanoparticles (200 nm dia.). In type iii, the Ag-s nanoparticle could be trapped near a large Ag particle in both positive (e.g., at 14.02 s) and negative (e.g., at 16.68 s) y directions. The two particles even jump or rotate around the chain axis; the Ag-s particles simultaneously move or jump between the two y-shifted positions. (See the Supporting Information Movie S6 and Figure S5 for an example of three Ag-s particles that orbit about the chain axis.) Other classes of co-trapping behaviors of small Ag nanoparticles are given in the Supporting Information, where Movie S7 and Figure S6 shows co-trapping of small Ag nanoparticles near large ones and Movie S8 and Figure S7 in the Supporting Information show intermediate-scale co-trapping. The spring constant for optical binding of the small and large Ag nanopartcles is ∼10 pN/μm.

While the near-field and intermediate-scale co-trapping of Ag-s nanoparticles share similarities with what we show above for QDs, there is also an important difference. Although the 60 nm Ag nanoparticles are small, they still scatter a significant amount of light, and that, in turn, affects the chain of large Ag nanoparticles: First, comparing the separations of particles Ag 2 and Ag 3 in regime (i) versus (ii or iii) shows that this separation is affected by the interstitial location of Ag-s. The Ag−Ag optical binding interaction is modified by the location of Ag-s. Second, by analyzing many optical bound Ag nanoparticle chains including the results in Figure 3, we conclude that there is a center of mass to the chains of metal nanoparticles. Adding a large particle to one end shifts the entire chain (along the long axis) so as to center this "center of optical binding" mass in the optical line trap. This effect is also noticeable but less pronounced for the smaller Ag nanoparticles. As seen in Figure 3b, the center of the chain shifts once the Ag-s changes positions. Both behaviors are in contrast with the co-trapped QDs, which behave as if they are transparent to the trapping laser and have negligible influence on the optically bound Ag particle chain.

The experimental results for semiconductor QDs co-trapped into an optically bound lattice of Ag nanoparticles showed that there are two regimes of localization: an intermediate scale where the QDs are between the Ag nanoparticles and a near-field regime where they are in close proximity to the Ag nanoparticles. Co-trapping of small Ag nanoparticles exhibits these similar behaviors as well. We performed 3D electrodynamics simulations using the finite-difference time-domain (FDTD) method to model the distribution of the EM fields around the chains of optically bound Ag nanoparticles and to understand the experimental results.

Figure 4a shows the 3D EM field distribution around two particles. Ag spheres (diameter 140 nm) in water are aligned along the x axis with separations of 564 nm and illuminated by a linearly polarized plane wave with λ = 800 nm. The light propagates in the z direction with polarization along the y axis. It is clear that interference from the coherent scattering of the particles creates a localized EM spot in the middle of their x positions and ∼200 nm away from their z positions (back toward the incoming field). As depicted in the cross-section of the x−z plane at y = 0, these light fields are nearly periodically spaced. Adding more particles into the chain creates more localizing EM spots, as shown in Figure 4b; these spots align in an array parallel to the chain, but their intensities vary with position. They are symmetric to the midplane of the chain and decrease in intensity toward the ends of the chain. (See the Supporting Information for more discussion.) The intensities of these features also depend on the number of particles in the chain. Adding particles to the end increases the intensities of all the spots.

Besides these localized EM spots, excitation of the plasmon resonance of the Ag nanoparticles will also produce strong EM fields near their surfaces as shown in Figure 4c. The particle plasmon is (weakly) excited by the incident and scattered electric fields associated with optical binding. This near-field enhancement oscillates along the polarization direction (i.e., the y axis). The EM fields are symmetric to and stronger near the midplane of the chain, indicating that the plasmon resonance enhancement is also enhanced by coherent scattering from all Ag nanoparticles. Note that for the present case the plasmon is only weakly excited because the 800 nm light is far to the red of the plasmon resonance maximum.

Figure 4d shows the particle number (N) dependence of the maximum intensities of the localized EM fields (red squares) and for the plasmon resonance-enhanced fields in a plane 20 nm away from the particle surface (green circles). In general, both intensities increase with particle numbers in the chain, but the plasmonic fields are stronger than the localized EM fields by ∼6-fold. The maximum intensities of the intermediate-scale localized EM fields increase sublinearly with the particle number. This reflects the slow (but finite) distance dependence of the optical binding effect.[24,29] As indicated by Figure 4e, a route to further increase the intensities of localized light fields is by using larger particles in the chain; the intensities increase rapidly with the particle diameters. Therefore, optically binding with more strongly scattering metal nanoparticles will allow co-

dx.doi.org/10.1021/jz401007t | J. Phys. Chem. Lett. 2013, 4, 2630−2636

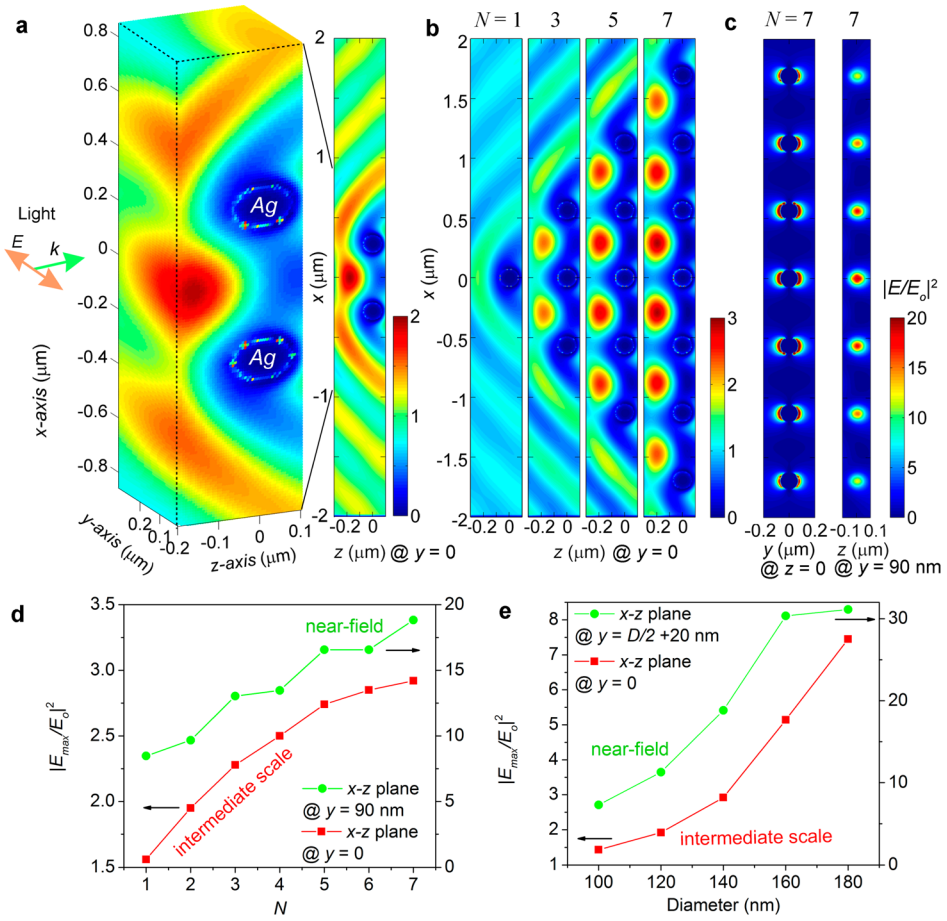

Figure 4. FDTD simulation of optical-field distributions around linear chains of Ag nanoparticles. (a) 3D EM field distribution around two particles. A cross-section of the $x-z$ plane at $y = 0$ is shown on the right. (b) Localized light fields created by linear chains with different number (N) of Ag nanoparticles. The panels are cross sections of the $x-z$ plane at $y = 0$. (c) Near-field EM field enhancement by plasmon resonance of Ag nanoparticles. The panels are cross sections of the $y-z$ plane at $y = 0$ and the $x-z$ plane at $y = 90$ nm. (d) Dependence of maximum field intensities ($|E/E_o|^2$, where E_o is the incident field) on the number of particles in the linear chains. (e) Dependence of maximum field intensities on the particle diameter ($N = 7$). In the last two panels, red squares are data for the localized light fields in the intermediate-length scale (i.e., the red spots in panel b) and green circles are data for the near-field at 20 nm away from the particle surfaces along the polarization direction.

trapping in metal nanoparticle lattices with fewer particles or stronger co-trapping with the same number of particles.

The simulations provide valuable insights into understanding the experimental results. On the basis of the trapping positions, near-field co-trapping is related to the plasmon-resonance-enhanced light fields, and intermediate-scale co-trapping is due to the localized EM "hot" spots. In the experiments, the optical images are a projection of the $x-y$ plane shown in Figure 4a, so a particle trapped by the localized spots will appear between two particles. Because the plasmonic fields are stronger, it is expected that the near-field co-trapping would be more likely to happen, and this is consistent with our experimental observations. However, the probability of co-trapping also depends on the integral of the intensity over space (the trapping volume). The plasmon resonance is a near-field effect, so the intensity will decay quickly (exponentially) with increasing distance from the particle surface. In contrast, the intermediate-scale localized EM spots are relatively weaker, but their volume is larger, which increases the probability of particle capture. Moreover, their intensities increase with Ag particle numbers in the chain, so the intermediate-scale co-trapping of QDs was typically only observed with seven or more Ag particles in Figures 1 and 2. Longer 1D optically bound arrays would enhance the intermediate scale co-trapping, as would the formation of 2D optically bound arrays because these increase the spatial density of scattering units and number of nearest neighbors to a given EM hot spot.

We have shown an intriguing bottom-up approach to creating "structured light" on subwavelength and near-field scales that enables hybrid assembly in a self-organizing manner using simple incident optical fields. We demonstrated that optically bound chains of Ag nanoparticles can create localized electromagnetic fields on intermediate scales near the chain and also enhance the plasmon resonance and the associated EM field in the near-field. These light fields allow co-trapping of semiconductor QDs and smaller Ag nanoparticles. The hierarchical optical binding has a superficial similarity to chemical bonding; however, the Coulomb interactions in the latter are replaced by spatially patterned EM fields and the attractive and repulsive interactions are electrodynamic. Our work represents a new all-optical approach to synthesize hybrid assemblies and the prospect to "engineer" coherence into synthetic nanophotonic systems. Novel quantum-optical and nonlinear-optical properties are expected from these hybrid assemblies. The localized light fields may also find applications in biology and photochemistry, and deposition of the Ag nanoparticle chains on a substrate will make the assemblies more robust for various applications that involve and benefit

dx.doi.org/10.1021/jz401007t | J. Phys. Chem. Lett. 2013, 4, 2630−2636

from field enhancement,[22,33,34] such as sensing (including SERS[35]), photocatalysis, and enhanced fluorescence from labeled biomolecules.

METHODS

Dynamic self-assembly of Ag nanoparticles was performed using an optical tweezers apparatus. Details of the apparatus were previously described.[11,36] An optical line trap was created via phase modulation of a Gaussian beam with laser power of 100 mW at the objective. Ag nanoparticles dispersed in water were trapped by the optical line (over 10 μm in length with linear polarization perpendicular to the line direction to achieve strong optical binding[24]) in a sample cell consisting of a spacer with a chamber between two coverslips. The Ag nanoparticles (with polyvinylpyrrolidone coating) were synthesized via a polyol route[29] but with doubled concentrations of reactants aiming to produce larger particles. The products were collected by centrifugation at 1000 rpm for 2 min. The average particle diameter is 140 nm with a standard deviation of 30 nm (see Supporting Information, Figure S1a).

To investigate the possibility of co-trapping in the optically bound chains of Ag particles, we mixed semiconductor QDs to the Ag particle solution in the sample cell. Commercial CdSe/ZnS core−shell QDs (coated with polyethylene glycol with thickness of ∼6 nm, the hydrodynamic size of the QDs is about 12−14 nm, purchased from Ocean NanoTech, #QMG620) and CdSe/CdZnS/SiO_2 QDs we synthesized[37] (the CdSe/CdZnS core size is about 7−9 nm, total size of the QDs is ∼40 nm) were used in the experiments. The former QDs emit fluorescence at 621 nm, and the latter emit at 600 nm (see Supporting Information, Figure S1b,c). To excite the fluorescence, we coupled a diode laser (Spectra-Physics Excelsior, operating at 488 nm) into the sample cell. This second laser was lightly focused to obtain a large illumination spot ∼15 μm in diameter and power of <10 mW. We verified that the 488 nm laser did not affect the optical binding interactions in the optical line trap.

To simultaneously image the QDs and the Ag nanoparticles with distinguishable positions, we used a "Dual-View" system (Photometrics DV2) to image them side by side with the same detector (Andor Neo sCMOS). Specifically, the recorded frame contains two regions: one region records only the orange/red fluorescence from the QDs, and the other one records only the dark-field scattered green light from the Ag nanoparticles. The positions of the Ag nanoparticles and the QDs were determined by a Gaussian centroid localization method[38] using commercial software (DiaTrack).

We also studied co-trapping of smaller Ag nanoparticles with the larger Ag nanoparticles in the optical line; in this case, monodisperse Ag nanoparticles of 60 nm diameters (with citrate coating, from Pelco NanoXact) were used and imaged with the green channel of the dual-view system.

Electrodynamics simulations were performed using Lumerical "FDTD Solutions" software. In the models, silver spheres with diameters of 140 nm are aligned along the x axis with separations of 564 nm, as specified by the most probable values from the present experiments (i.e., particle−particle separation distribution functions). The spheres are illuminated by a linearly polarized plane wave with λ = 800 nm (vacuum). The light propagates in the z direction with polarization along the y axis. A nonuniform mesh with maximum grid size of 5 nm was used. The dielectric function of Ag was modeled with the Johnson and Christy data,[39] and the background refractive index was set to be 1.33 (the infinite-frequency refractive index of water).

ASSOCIATED CONTENT

Supporting Information

Video clips showing the assembly of Ag nanoparticles, co-trapping of QDs and smaller Ag nanoparticles, and additional figures. This material is available free of charge via the Internet at http://pubs.acs.org.

AUTHOR INFORMATION

Corresponding Author

*E-mail: nfschere@uchicago.edu.

Notes

The authors declare no competing financial interest.

ACKNOWLEDGMENTS

This work was supported by the National Science Foundation (CHE-1059057). P.G.S. and W.Q. also acknowledge the NSF (CHE-1111799) for support. We acknowledge the University of Chicago NSF-MRSEC (DMR-0820054) for central facilities.

REFERENCES

(1) Mikhael, J.; Roth, J.; Helden, L.; Bechinger, C. Archimedean-Like Tiling on Decagonal Quasicrystalline Surfaces. *Nature* **2008**, *454*, 501−504.

(2) Talapin, D. V.; Shevchenko, E. V.; Bodnarchuk, M. I.; Ye, X.; Chen, J.; Murray, C. B. Quasicrystalline Order in Self-Assembled Binary Nanoparticle Superlattices. *Nature* **2009**, *461*, 964−967.

(3) Will, S.; Best, T.; Schneider, U.; Hackermueller, L.; Luehmann, D.-S.; Bloch, I. Time-Resolved Observation of Coherent Multi-body Interactions in Quantum Phase Revivals. *Nature* **2010**, *465*, 197−201.

(4) Dienerowitz, M.; Mazilu, M.; Dholakia, K. Optical Manipulation of Nanoparticles: a Review. *J. Nanophotonics* **2008**, *2*, 021875.

(5) Fazal, F. M.; Block, S. M. Optical Tweezers Study Life Under Tension. *Nat. Photonics* **2011**, *5*, 318−321.

(6) Svedberg, F.; Li, Z.; Xu, H.; Käll, M. Creating Hot Nanoparticle Pairs for Surface-Enhanced Raman Spectroscopy through Optical Manipulation. *Nano Lett.* **2006**, *6*, 2639−2641.

(7) Čižmár, T.; Romero, L. C. D.; Dholakia, K.; Andrews, D. L. Multiple Optical Trapping and Binding: New Routes to Self-Assembly. *J. Phys. B: At., Mol. Opt. Phys.* **2010**, *43*, 102001.

(8) Neuman, K. C.; Block, S. M. Optical Trapping. *Rev. Sci. Instrum.* **2004**, *75*, 2787−2809.

(9) Grier, D. G. A Revolution in Optical Manipulation. *Nature* **2003**, *424*, 810−816.

(10) Padgett, M.; Bowman, R. Tweezers with a Twist. *Nat. Photonics* **2011**, *5*, 343−348.

(11) Yan, Z.; Jureller, J. E.; Sweet, J.; Guffey, M. J.; Pelton, M.; Scherer, N. F. Three-Dimensional Optical Trapping and Manipulation of Single Silver Nanowires. *Nano Lett.* **2012**, *12*, 5155−5161.

(12) Yang, A. H. J.; Moore, S. D.; Schmidt, B. S.; Klug, M.; Lipson, M.; Erickson, D. Optical Manipulation of Nanoparticles and Biomolecules in Sub-Wavelength Slot Waveguides. *Nature* **2009**, *457*, 71−75.

(13) Grigorenko, A. N.; Roberts, N. W.; Dickinson, M. R.; Zhang, Y. Nanometric Optical Tweezers Based on Nanostructured Substrates. *Nat. Photonics* **2008**, *2*, 365−370.

(14) Righini, M.; Volpe, G.; Girard, C.; Petrov, D.; Quidant, R. Surface Plasmon Optical Tweezers: Tunable Optical Manipulation in the Femtonewton Range. *Phys. Rev. Lett.* **2008**, *100*, 186804.

(15) Ploschner, M.; Cizmar, T.; Mazilu, M.; Di Falco, A.; Dholakia, K. Bidirectional Optical Sorting of Gold Nanoparticles. *Nano Lett.* **2012**, *12*, 1923−1927.

(16) Guffey, M. J.; Miller, R. L.; Gray, S. K.; Scherer, N. F. Plasmon-Driven Selective Deposition of Au Bipyramidal Nanoparticles. *Nano Lett.* **2011**, *11*, 4058−4066.
(17) Juan, M. L.; Righini, M.; Quidant, R. Plasmon Nano-Optical Tweezers. *Nat. Photonics* **2011**, *5*, 349−356.
(18) Zhang, W.; Huang, L.; Santschi, C.; Martin, O. J. F. Trapping and Sensing 10 nm Metal Nanoparticles Using Plasmonic Dipole Antennas. *Nano Lett.* **2010**, *10*, 1006−1011.
(19) Pang, Y.; Gordon, R. Optical Trapping of a Single Protein. *Nano Lett.* **2012**, *12*, 402−406.
(20) Pauzauskie, P. J.; Radenovic, A.; Trepagnier, E.; Shroff, H.; Yang, P. D.; Liphardt, J. Optical Trapping and Integration of Semiconductor Nanowire Assemblies in Water. *Nat. Mater.* **2006**, *5*, 97−101.
(21) Benson, O. Assembly of Hybrid Photonic Architectures from Nanophotonic Constituents. *Nature* **2011**, *480*, 193−199.
(22) Lin, S.; Zhu, W.; Jin, Y.; Crozier, K. B. Surface-Enhanced Raman Scattering with Ag Nanoparticles Optically Trapped by a Photonic Crystal Cavity. *Nano Lett.* **2013**, *13*, 559−563.
(23) Burns, M. M.; Fournier, J. M.; Golovchenko, J. A. Optical Binding. *Phys. Rev. Lett.* **1989**, *63*, 1233−1236.
(24) Dholakia, K.; Zemánek, P. Colloquium: Gripped by Light: Optical Binding. *Rev. Mod. Phys.* **2010**, *82*, 1767−1791.
(25) Karasek, V.; Cizmar, T.; Brzobohaty, O.; Zemanek, P.; Garces-Chavez, V.; Dholakia, K. Long-Range one-Dimensional Longitudinal Optical Binding. *Phys. Rev. Lett.* **2008**, *101*, 143601.
(26) Whitesides, G. M.; Grzybowski, B. Self-Assembly at All Scales. *Science* **2002**, *295*, 2418−2421.
(27) Demergis, V.; Florin, E.-L. Ultrastrong Optical Binding of Metallic Nanoparticles. *Nano Lett.* **2012**, *12*, 5756−5760.
(28) Dienerowitz, M.; Mazilu, M.; Reece, P. J.; Krauss, T. F.; Dholakia, K. Optical Vortex Trap for Resonant Confinement of Metal Nanoparticles. *Opt. Express* **2008**, *16*, 4991−4999.
(29) Yan, Z.; Shah, R. A.; Chado, G.; Gray, S. K.; Pelton, M.; Scherer, N. F. Guiding Spatial Arrangements of Silver Nanoparticles by Optical Binding Interactions in Shaped Light Fields. *ACS Nano* **2013**, *7*, 1790−1802.
(30) Jin, R. C.; Jureller, J. E.; Scherer, N. F. Precise Localization and Correlation of Single Nanoparticle Optical Responses and Morphology. *Appl. Phys. Lett.* **2006**, *88*, 263111.
(31) Bohren, C. F.; Huffman, D. R. *Absorption and Scattering of Light by Small Particles*; Wiley-VCH Verlag GmbH: Weinheim, Germany; 2007.
(32) Jauffred, L.; Oddershede, L. B. Two-Photon Quantum Dot Excitation During Optical Trapping. *Nano Lett.* **2010**, *10*, 1927−1930.
(33) Li, J. F.; Huang, Y. F.; Ding, Y.; Yang, Z. L.; Li, S. B.; Zhou, X. S.; Fan, F. R.; Zhang, W.; Zhou, Z. Y.; Wu, D. Y.; et al. Shell-Isolated Nanoparticle-Enhanced Raman Spectroscopy. *Nature* **2010**, *464*, 392−395.
(34) Le, F.; Brandl, D. W.; Urzhumov, Y. A.; Wang, H.; Kundu, J.; Halas, N. J.; Aizpurua, J.; Nordlander, P. Metallic Nanoparticle Arrays: A Common Substrate for Both Surface-Enhanced Raman Scattering and Surface-Enhanced Infrared Absorption. *ACS Nano* **2008**, *2*, 707−718.
(35) Ko, H.; Singamaneni, S.; Tsukruk, V. V. Nanostructured Surfaces and Assemblies as SERS Media. *Small* **2008**, *4*, 1576−1599.
(36) Yan, Z.; Sweet, J.; Jureller, J. E.; Guffey, M. J.; Pelton, M.; Scherer, N. F. Controlling the Position and Orientation of Single Silver Nanowires on a Surface Using Structured Optical Fields. *ACS Nano* **2012**, *6*, 8144−8155.
(37) Koole, R.; van Schooneveld, M. M.; Hilhorst, J.; Donega, C. d. M.; t Hart, D. C.; van Blaaderen, A.; Vanmaekelbergh, D.; Meijerink, A. On the Incorporation Mechanism of Hydrophobic Quantum Dots in Silica Spheres by a Reverse Microemulsion Method. *Chem. Mater.* **2008**, *20*, 2503−2512.
(38) Qu, X. H.; Wu, D.; Mets, L.; Scherer, N. F. Nanometer-Localized Multiple Single-Molecule Fluorescence Microscopy. *Proc. Natl. Acad. Sci. U.S.A.* **2004**, *101*, 11298−11303.
(39) Johnson, P. B.; Christy, R. W. Optical Constants of the Noble Metals. *Phys. Rev. B* **1972**, *6*, 4370−4379.